PERGAMON

Journal of Structural Geology 23 (2001) 745–763

JOURNAL OF STRUCTURAL GEOLOGY

www.elsevier.nl/locate/jstrugeo

Fault growth by linkage: observations and implications from analogue models

Chris Mansfield[a,*], Joe Cartwright[b]

[a]Nederlandse Aardolie Maatschappij B.V., Business Unit Offshore, Grote Hout of Koningsweg 49, 1950 AA, Velsen-Noord, The Netherlands
[b]Department of Earth Sciences, P.O. Box 914, University of Cardiff, Cardiff CF10 3YE, UK

Received 14 June 1999; accepted 19 July 2000

Abstract

Using time sequence analyses of extensional fault models we demonstrate the pivotal role played by fault segmentation in the accumulation of displacement and length during the growth of faults. Experiments are described in which incremental steps during the development of individual faults have been reconstructed from time-lapse photographs taken during model deformation. These records confirm the composite segment hierarchy of fault structure, a pattern that is frequently recognised in many natural arrays. They reveal the progressive enlargement of individual faults to be the product of a repetitive cycle of tip-line propagation, overlap and linkage between nearest neighbours. By contrasting the displacement patterns of successive increments during growth convincing evidence is also presented to suggest that individual segments of faults may remain kinematically independent once they are physically linked. This behaviour is shown to be responsible for the characteristic saw-tooth patterns often recognised in strike-parallel fault displacement profiles. Such patterns are believed to arise where relict segment boundaries remain preserved as asperities to slip, so that displacement is confined to discrete parts of a fault plane surface.

Growth in this way also causes the maximum displacement (D) and surface length (L) of faults to continually change by different proportions. Incremental displacement records presented here corroborate field evidence which shows that linkage between fault segments during growth is responsible for a significant component of the spread of values often recorded in D versus L compilations. Finally, we speculate that linkage between fault segments also accounts for transient irregularities recorded in the frequency distribution of the fault length populations of each model. © 2001 Elsevier Science Ltd. All rights reserved.

1. Introduction

Field evidence suggests that the segmented structure of faults is a fundamental characteristic of most natural arrays across a very wide range of scales. Such prevalence points to a central role for linkage between segments as an important building block in the growth of faults. Yet, current understanding of its significance in fault growth remains a limited and largely piecemeal interpretation of a variety of isolated and diverse fault systems.

Direct evidence for the role of segments during periods of fault growth activity is limited by the often lengthy repeat times between individual fault slip events. As a result, most published interpretations are based largely on interpolating between field examples that are believed to represent discrete stages in the process of segment linkage. Increasingly sophisticated theoretical models have been developed as an alternative approach to understanding long-term fault growth processes (Pollard and Segall, 1987; Cowie and Scholz, 1992a,b; Cowie et al., 1993; Bürgmann et al., 1994; Willemse et al., 1996; Cowie, 1998), but these frequently incorporate highly simplified assumptions regarding the mechanical behaviour of the fractured media and the boundary conditions governing deformation.

Present understanding of the role of fault segmentation therefore continues to be shrouded by considerable uncertainty. Its influence on the accumulation of displacement and length during growth remains widely debated. Most recent views have polarised around two conflicting interpretations of the proportions and the timing by which the maximum displacement (D) and length (L) of fault segments increase during linkage. Data presented in favour of progressive increases in values of D/L during fault segment interaction and linkage (Dawers and Anders, 1995; Nicol et al., 1996; Peacock and Sanderson, 1996) are apparently contradicted by measurements suggesting deviations to

* Current address: Shell Capital Services Ltd, Shell Centre, London SE1 7NA, UK.

0191-8141/01/$ - see front matter © 2001 Elsevier Science Ltd. All rights reserved.
PII: S0191-8141(00)00134-6

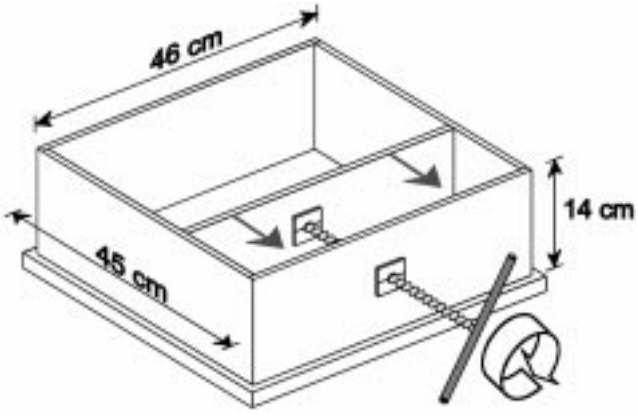

Fig. 1. Schematic illustration of the apparatus used in each of the modelling experiments. The Crystacal plaster and barite mud were layered in the rear half of this box. Subsequent forward movement of the internal confining wall (in the direction indicated) was driven by a worm screw connected to an external handle, as shown.

lower values (Filbrandt et al., 1994), but are partially reconciled by elements of each in a model presented by Cartwright et al. (1995).

Establishing the effects of segment linkage on fault displacement distributions is important for understanding both short-term and long-term fault scaling behaviour, and for constraining spatial and temporal patterns of earthquake activity in segmented fault systems. In turn, this underpins our interpretation of the impact on a variety of secondary processes, including the evolution of surface drainage patterns, the development and switching of fault controlled depocentres and the geometry of syn-rift sedimentary bodies.

In this paper we describe the results of a series of modelling experiments in which gravitational collapse of a layered plaster and barite mud sequence has been used as an analogue for the development of extensional fault systems. Measurements recorded from time-lapse photographs taken during the experiments are used to assess the structural and displacement evolution of individual faults. In this way, fault geometries and displacements measured at the end of extension can be interpreted in the context of temporal changes in fault development seen during model extension. The results describe in detail the changing relationship between the maximum displacement and strike length of faults during growth. They have also enabled incremental changes in the fault length frequency distributions of selected populations to be examined in detail. This careful time-lapse approach to the study of fault growth has emphasised the dynamic over the static, and in so doing has underscored the fundamental role played by segment linkage in fault growth. We therefore conclude this paper with a discussion of some of the implications that these plaster-modelling experiments have for our understanding of fault linkage processes and in particular for the scaling of maximum displacement and fault length during growth.

2. Methodology

2.1. Modelling rationale

Scaled physical modelling is an established, well-documented technique that provides for fully balanced, reproducible simulations (Hubbert, 1937; Oertel, 1965; Vendeville et al., 1987). The particular application of Crystacal plaster as a modelling material is less conventional, but its successful use is well described by Sales (1987) and by Fossen and Gabrielsen (1996). We prefer it to dry quartz sand because its finer grain size provides for a much wider range of discernible fault sizes, and it has the added advantage of producing robust, solid models. Also, in common with clay modelling its relatively high cohesive strength results in finite amounts of distributed ductile strain during early extension (Naylor et al., 1986). Analogous ductile folding in nature has been recognised in many strained regions of the Earth's crust, and is believed often to occur as a precursor to brittle failure (Ramsay and Huber, 1987).

For materials obeying Navier-Coulomb failure criterion, accurate scaling requires that the model and real earth cohesive strengths should scale in the same proportion as the ratio of their unit thickness (Horsfield, 1977). Laboratory replications of crustal scale faulting therefore require a near cohesionless medium (McClay and Ellis, 1987; Naylor et al., 1993). At the time of deformation our plaster mixture possessed a relatively high cohesive strength, exemplified by its tendency to produce tensile micro-fractures under small, early extensional strains. Our models are therefore more strictly representative of smaller scale near-surface faulting and, we believe, represent good analogues for extensional fault arrays such as described in the Canyonlands (Cartwright et al., 1995, 1996) and the Volcanic Tablelands (Dawers et al., 1993; Dawers and Anders 1995). However, since the structural and displacement characteristics associated with faulting and segment linkage are often scale independent (Tchalenko, 1970; Nelson et al., 1992; Peacock and Sanderson 1994; Peacock 1995) we expect that the results presented below are likely to be significant for faulting across a range of scales.

In the experiments described here, continued rheological changes related to hardening of the plaster during extension are considered negligible. Although a certain variability from one experiment to another is anticipated, the 20 to 30 s duration of individual model runs is small in comparison to the 1 h required for complete solidification of the plaster. The effects of rheological changes were similarly dismissed by Fossen and Gabrielsen (1996), as they were able to show that the angle of internal friction during their plaster experiments varied only within small limits.

2.2. Experimental procedure

Nine experiments are described below (Models 33 to 41). In each, gravitational spreading of a two-layer Crystacal

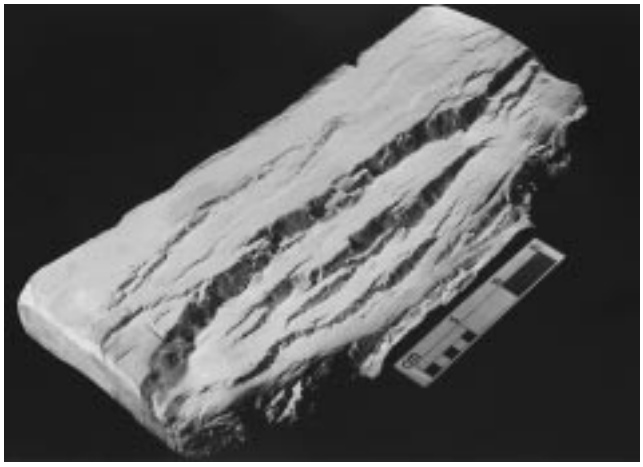

Fig. 2. Photograph showing Model 38 at the end of extension. The faults at surface are sharp and well defined, and exhibit dips in the range 65–90°. Low angle lighting applied from the rear of the model (top left corner) emphasises the predominantly sub-parallel alignment of the faults, arranged in sub-parallel, synthetic sets that dip in the direction of extension and bound partially rotated domino fault blocks. Most of the faults are complex, composite structures comprised of a series of overlapping, linked and unlinked fault segments.

plaster and barite mud sequence was used to simulate extensional deformation of a brittle overburden with a ductile substrate. The apparatus used in these experiments was an open-topped wooden box with a moveable internal wall (Fig. 1). At the start of each experiment the plaster and barite mud were layered in approximately equal thickness, of about 4–5 cm, in one half of this box. Subsequent hardening of the plaster was monitored by miniature slump tests at the model edges, and extension was initiated once the plaster had reached the consistency of a thick syrup. A uniform outward (extensional) movement was applied to the internal wall by a worm screw connected to an external handle, at a rate of approximately 0.5 cm/s^{-1}. In response to gravity, the plaster spread towards the unwinding wall under its own body weight, the surface usually deforming into a series of discrete, tilted fault blocks.

Studies of incremental changes to the structural and displacement geometries of the faults during growth were enabled with time-lapse photography, using a 35 mm camera angled at 70° to the horizontal. Each model run lasted between 20 and 30 s, and each was recorded with photographs at half-second increments.

2.3. Model deformation

Surface fault patterns in all of the models were conditioned by the early nucleation and growth of precursor microfractures, each of which appeared to develop with purely tensile-opening displacements. The development of these tensile microfractures was apparently random, and probably governed by points of weakness caused by inhomogeneities within the plaster mix (c.f. Lachenbruch, 1962). The speed of model deformation prevented reliable recognition of the moment at which shear displacements were resolvable on the microfractures, or if the onset of shear was related to a critical fracture dimension or amount of strain. However, once shear displacements had been initiated, little or no further tensile displacements were apparent during subsequent growth.

Increased displacements on the faults were accompanied by a simultaneous propagation of the respective lateral tips. Since fault propagation was generally perpendicular to the extension direction, many with proximal nucleation positions eventually reached positions of overlap. Subsequent physical connection was subject to breaching of the relay ramp between them. In this way, composite linked structures were established from previously discrete and structurally isolated fault segments. This repetitive cycle of propagation, overlap and linkage was characteristic of the lengthening of all faults in the plaster models, and resembles the interpretation advanced by Cartwright et al. (1995) for the evolution of a multi-segmented fault array in the Canyonlands, Utah.

Faults in the solidified models at the end of extension (Fig. 2) exhibit many of the geometrical and displacement characteristics commonly recognised in natural extensional fault systems (Peacock and Sanderson, 1991; Anders and Schlische, 1994; Cartwright et al., 1995, 1996; Dawers and

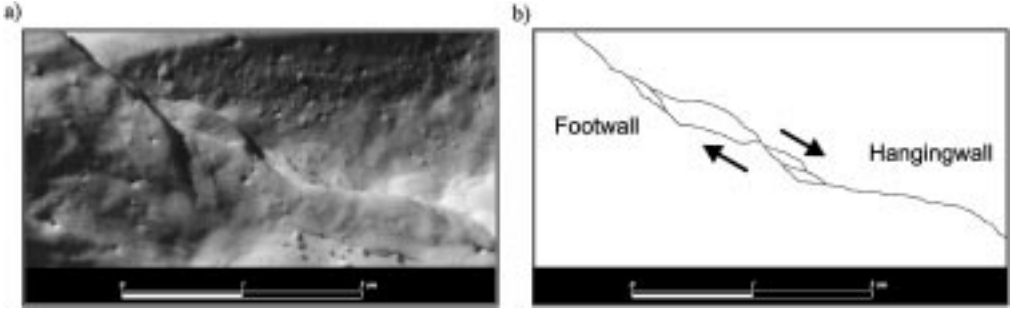

Fig. 3. (a) Photograph, and (b) line drawing interpretation, of a fault exposed in cross-section along one edge of Model 33. The complex overlapping and branching geometry of the slip plane evident here attests to a history of growth governed by the independent propagation of precursor fault segments throughout the thickness of the plaster layer.

Anders, 1995). Faults at all scales exist not as single elements but as composite structures, composed of an amalgamated hierarchy of smaller linked and unlinked segments. Relay ramps between fault segments overlapping along strike exhibit many contrasting geometries, that represent different stages in a cycle of growth by segment linkage. Each model demonstrates a progression from discrete, en echelon structures with varying degrees of overlap, to embryo and mature linkages between large fault segments offset across breached relay ramps.

The faults in each model exhibit a wide range of displacements. Those with the largest displacements cut the entire thickness of the plaster layer. Inspection of the underside of the models indicates that these largest faults are planar to moderately listric and detached on or within the top of the barite mud substrate. Clear exposures of the fault planes in cross section, at the model edges (Fig. 3), suggest that fault evolution in the slip direction was largely analogous to that along strike. That is, fault development was governed by coalescence between early isolated, small faults that propagated upwards and downwards through the plaster layer. They probably evolved with a moderately listric geometry as a consequence of coalescing inclined shears at depth with vertical tension fractures and subvertical hybrid shears at the upper free surface. Fault block rotation during extension is also expected to have induced a small component of contemporaneous fault plane rotation. Observations that early surface deformation was accompanied by the formation of shear fractures at depth have also been reported by Fossen and Gabrielsen (1996), following similar extensional plaster and barite mud experiments.

2.4. Fault Measurements

Fault lengths and displacements were recorded by taking measurements directly from selected well-defined examples in the time-lapse photograph sets. For a number of faults in each model, this enabled patterns of incremental change to be established at regular intervals during growth. Calibration of these measurements was ensured by recording final geometries from the same faults in each of the solid models.

The faults selected for analysis were those that did not intersect the boundary walls and that clearly were not influenced by any adjacent frictional drag effects. This excluded all those faults wholly or partially within an area approximately 3 cm wide parallel to the boundary walls, within which there was distinct curvature of the fault traces, concave in the direction of extension.

By definition, the measured faults have their upper tips at the free surface. Many of the largest dissected the entire thickness of the plaster layer. The measured lengths and displacements can therefore be expected to represent maximum values for the respective fault plane surfaces in each case (Barnett et al., 1987).

2.5. Fault displacements

Fault displacements were defined as the dip-slip displacement of the free surface, and were recorded both from the solid models and from the photographs using a millimetre scale. In each case displacements were directly observable, with the exception of a few of the very smallest faults in the photographs for which the shadow cast by high-angle overhead lighting was used as a proxy. To ensure that the detail of each distribution was preserved, measurements were taken at closely spaced intervals of between 0.5 and 1 cm along the strike of each of the faults. Results were then plotted as strike-parallel vertical projections for analysis and display.

2.6. Fault lengths

Fault lengths were recorded as the straight line distance separating two well defined lateral tips. In this respect, however, the arrangement of most faults as a hierarchy of individual linked and unlinked segments was problematic. No consensus currently exists as to the precise critical separation within which two neighbouring segments constitute a single fault structure (Gudmundsson, 1987a,b; Bilham and Bodin, 1992; Mansfield, 1996). For the purposes of comparison and discussion, two separate fault length measurements were therefore recorded. In the first instance, measurements included only those fault segments for which there was an unequivocal, physical connection of the respective slip planes at surface (‘hard-linkage’). In the second case, measurements included adjacent fault segments kinematically linked by deformation of the material volume between them (‘soft-linkage’). Based on concepts of elastic interaction (Huggins et al., 1995; Willemse et al., 1996), criteria in the latter case required the tips of fault segments to be overlapping, and to be separated perpendicular to strike by a distance equivalent to less than half the fault surface trace lengths.

2.7. Errors

Measurement accuracy achieved with the millimetre scale is estimated to be ± 0.5 mm. Calibration between the final time-lapse photograph in each set and the respective solid model confirmed that measurements recorded from the photographs are accurate to about 1 mm. The measurement of shadow, as a proxy for the displacements of the very smallest faults in the time-lapse photographs, is expected to have introduced additional error. However, this error is considered to be small because the faults at surface are subvertical and the lighting was applied at a very high angle. A small, but unquantified, error was also incurred by defining fault length as a straight line distance, as almost all faults in the plaster models exist as composite segmented structures and in some cases also exhibit mildly arcuate surface trace geometries.

In general, the errors described above resulted either from

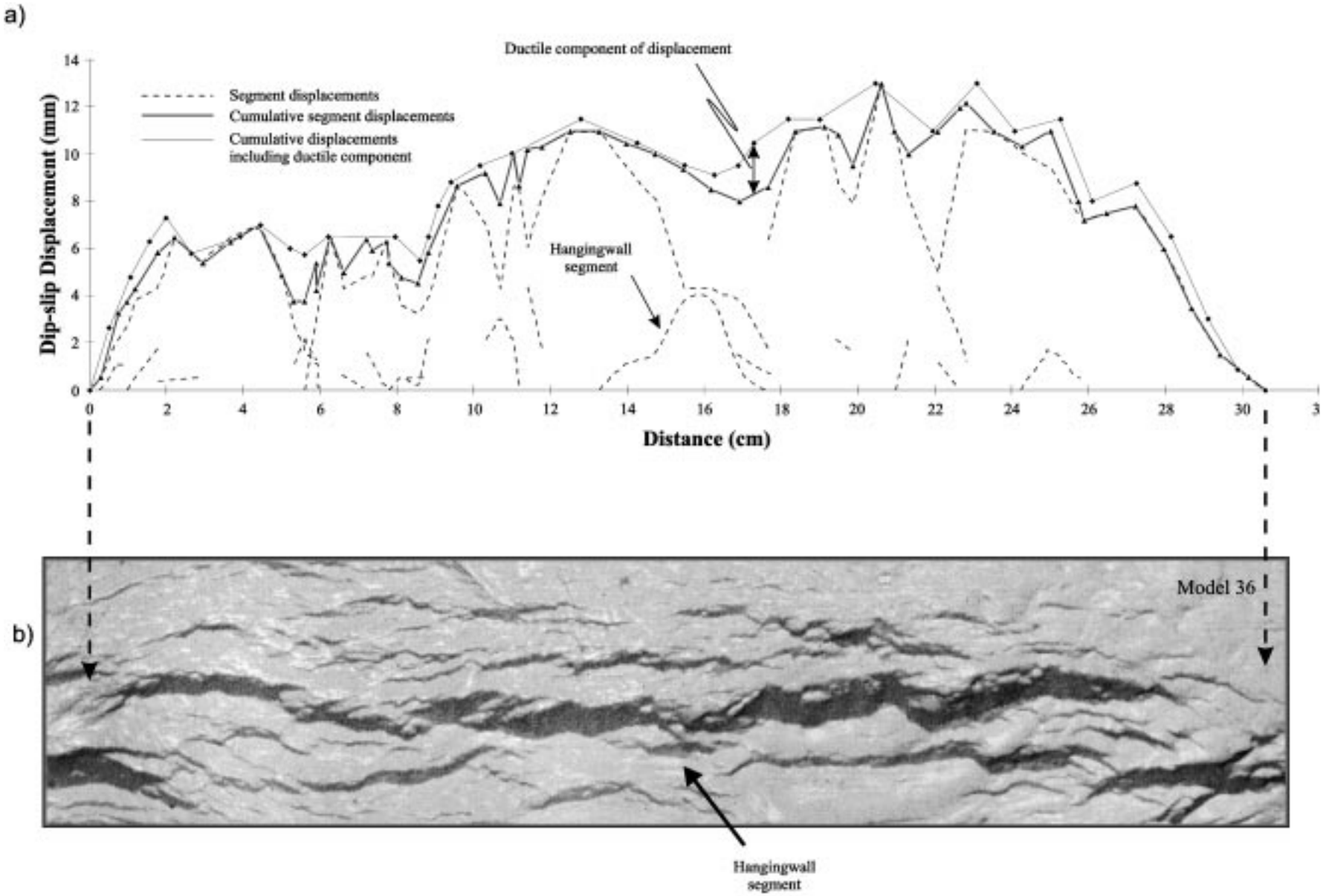

Fig. 4. (a) Strike-parallel profile showing dip-slip displacements recorded at discrete intervals along a large segmented fault in Model 36. The accompanying cumulative profiles describe the sum of displacements at overlapping segments and splays, respectively excluding and including the fault-related continuous ('ductile') component of displacement. (b) Plan-view photograph showing the corresponding surface geometry of the fault. The model is illuminated by low-angle lighting from the rear (top of photograph) so that the fault planes are cast in shadow.

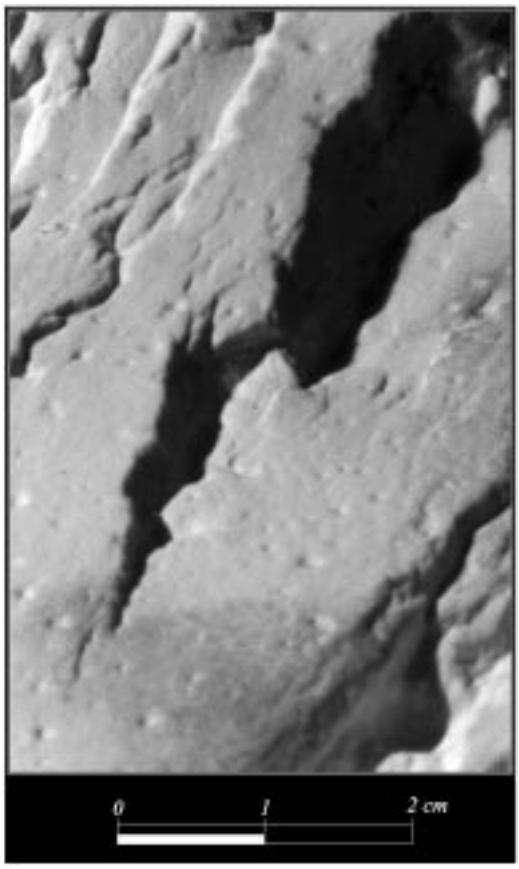

Fig. 5. Photograph showing the clarity of definition typical at the lateral tips of faults in the plaster models. Overhead lighting to the left of the picture has cast shadow from the planes of those faults that downthrow to the right.

the resolution limits of the time-lapse photographs or from the accuracy that could be achieved with a millimetre scale. We therefore expect that the measurement errors will be proportionately larger for the very smallest faults in each population.

3. Results

3.1. Displacement profiles

Large displacement variations are evident along the strike of faults in all of the solid plaster models at the end of extension. Features typical of the recorded displacement profiles are illustrated in Fig. 4, which shows a large multi-segmented fault along which all of the segments are hard-linked across breached relay ramps.

Component segments of the fault are evident as separate culminations in the displacement profile, each with steep gradients towards interjacent relay ramps (Peacock and Sanderson, 1991). In the region of overlapping segment tips the sum of displacements is generally less than on adjacent parts of the fault surface. The cumulative profile therefore describes a moderately irregular but approximately flat-topped distribution, fluctuating between a series of local displacement maxima at segment centres and minima at segment boundaries.

The association between fault displacement minima and the conjunction of neighbouring segment tips is well recognised. Observations have been documented from a number of natural fault systems, both for overlapping, soft-linked fault segments and also for segments hard-linked across breached relay ramps (Machette et al., 1991; Peacock and Sanderson, 1991, 1994; Dawers et al., 1993; Trudgill and Cartwright, 1994). It is argued that such displacement minima may largely be accounted for by the ductile component of deformation within the relay ramp, between the overlapping fault segment tips (Peacock and Sanderson, 1991; Dawers and Anders, 1995). In order to test this idea, the topographic separation of footwall and hangingwall along the strike of the fault presented in Fig. 4 was measured from the model. The resulting profile (Fig. 4) includes both the continuous and discontinuous components of displacement. When compared with the original cumulative

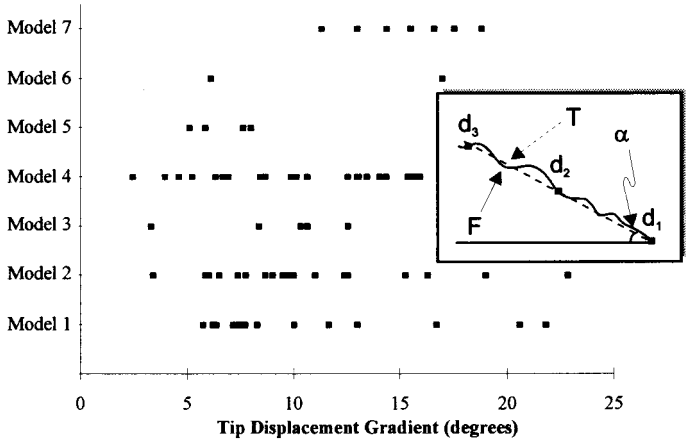

Fig. 6. Lateral tip displacement gradients recorded from faults in seven plaster models. Inset shows how individual displacement gradients (α) were established on the basis of a lateral taper approximation (T) of fault dip-slip displacement (F), determined from discrete measurements of the footwall and hangingwall separation (d). Frictional drag effects at the apparatus edges and interaction between neighbouring faults meant that reliable definition of an accurate gradient was possible only for a limited number of faults in each model.

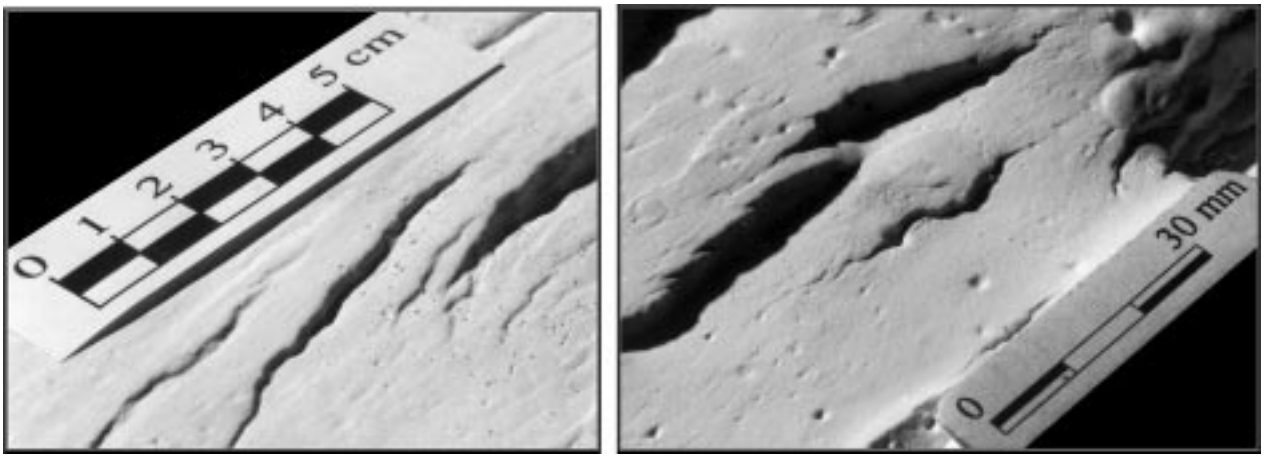

Fig. 7. Oblique-angle photographs showing the variability of relay ramp geometries between overlapping segments of faults in the plaster models. Most are sub-rectangular, bounded generally by faults that are parallel. The ramps exhibit a wide range of dips and may also be faulted internally before being completely breached.

displacement profile it is clear that a proportion of displacement is accommodated by ductile deformation at most places along the strike of the fault. In places, ductile deformation accounts for greater than 1 mm of offset, representing as much as 10% of the total displacement. Inclusion of the ductile element has substantially smoothed the displacement profile, most noticeably at the relay ramps. However, the remaining fluctuations in this displacement profile are clear evidence that ductile deformation has not completely accounted for the entire displacement deficit observed at every relay ramp.

3.2. Fault tip regions

The exposed lateral tips of many faults in the plaster models are exceptionally well defined (Fig. 5). Discrete displacement measurements recorded within each tip region show that in general the decrease in displacement along strike defines a uniform, linear taper. The acute angle between the footwall and the hangingwall cut-off then defines the tip displacement gradient. Careful measurements of this gradient at 75 lateral tips, from faults in seven models, reveals a wide range of values (Fig. 6). Rather than clustering about a median, the measured gradients define a continuous distribution from about 3° to 23°.

The wide range of recorded tip displacement gradients may be attributed to a variety of effects. Firstly, different rates of solidification within each model volume are likely to have resulted in spatial heterogeneities in the shear strength of the plaster around each fault tip and also variable cohesion along the established fault planes. Secondly, stress field interference between neighbouring faults is believed to be an important factor governing proximal tip displacement gradients (Bürgmann et al., 1994; Cartwright and Mansfield, 1998). However, the results of a numerical model presented recently by Cowie and Shipton (1998) suggest that the stress field beyond fault tips decays rapidly with distance, and that therefore this effect may be of limited influence. Since care was taken to ensure that measured tips of faults in the plaster models exceeded a minimum separation distance from nearest neighbours (Section 2.6) we consider the effect attributable here to fault interaction to be negligible. Finally, other potentially important considerations are spatial and temporal variations in the remote stress loading the faults (Bürgmann et al. 1994). Moderate changes may have been introduced by fluctuations in the applied extension rate and by variations in the flow of the underlying barite mud. We consider, however, that this explanation alone is unlikely to account for the order of magnitude variation in the measured tip gradients.

Whilst the effects described above are strictly applicable to fault growth in the plaster models, each represents a mechanical condition that can be expected to have a natural analogue. The arguments presented here particularly favour the importance of mechanical heterogeneities in shaping fault displacement geometries. Contrary to the implications of many theoretical models that consider isolated fault growth in homogeneous media (Pollard and Segall, 1987; Cowie and Scholz, 1992a,b), the growth of faults in natural arrays is unlikely to be characterised by a narrow range of tip displacement gradients. Rather, a wide spread of values is more likely, governed largely by the mechanical boundary conditions specific to each (Cartwright and Mansfield, 1998; Cowie and Shipton, 1998).

3.3. Relay ramp geometries

Propagation of lateral fault tip lines during model extension was typically perpendicular to the flow of plaster, resulting in sub-parallel propagation trajectories. Relay ramps between overlapping fault segments therefore exhibit a range of quasi-rectangular geometries, bounded by faults with variable tip displacement gradients (Fig. 7). Hard-linkage between fault segments was established either by

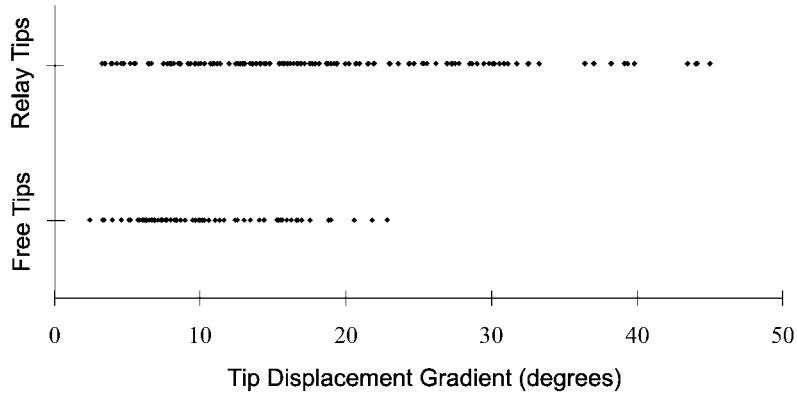

Fig. 8. Comparison between the range of displacement gradients recorded at the tips of faults in relay ramps with those at free lateral tips. See main text for discussion.

footwall or hangingwall breaching, or by connectivity at intermediate positions within the ramps. In this way the tips of one or both of the bounding fault segments were stranded as small splay faults in the footwall or hangingwall. Occasionally, examples were also found of 'double-breached' ramps, where linkage was achieved by both the footwall and the hangingwall fault segments.

The shear strains that govern relay ramp deformation are conditioned largely by displacement gradients at the overlapping tips of the bounding faults, and by the separation distances between them (Peacock and Sanderson, 1991, 1994). Where these properties are recorded from faults bounding breached relay ramps, they potentially provide a measure of the critical threshold conditions required to link two neighbouring faults. However, these properties may also change with time if slip continues to accumulate along the bounding splay faults once a relay ramp is breached. Objective assessment of the geometries and displacements likely to govern fault linkage based on present day observations of breached relay ramps in nature is therefore likely to be unreliable. In contrast, the use of time-lapse photography during the modelling experiments described here enabled the instant of relay ramp breaching to be recorded, and the fault displacements identified.

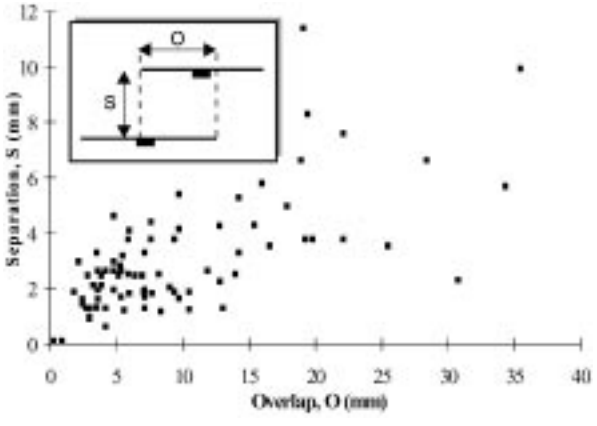

Fig. 9. Cross-plot of separation (S) versus overlap (O) distances recorded from 87 breaching relay ramps in five plaster models. (See inset for definition). The data broadly define a trend that relaying faults with wider separations have longer overlap lengths. Note, however, that there is a substantial spread of values at every dimension.

Strike parallel 'overlap' (O) and strike perpendicular 'separation' (S) distances, and the associated tip displacement gradients, were recorded from photographic coverage of 87 breaching relay ramps in five of the plaster models. Measurements were in each case recorded one photographic frame before nucleation of the first fault transecting a ramp, representing the instant before breaching of that ramp at surface.

Displacement gradients recorded at the overlapping tips span a range of values from 4° to 45° (Fig. 8) with most clustered between 4° and 34°. This cluster overlaps significantly with the range of gradients recorded at free tips, suggesting that in addition to fault interaction a number of other mechanisms play a role in controlling the displacement gradients of neighbouring tips. The influence of spatial and temporal variations in fault slip are considered of particular importance (Cowie and Shipton, 1998). This topic is addressed in a later section.

Relay ramps in the plaster models develop and subsequently breach between faults with quite different overlap lengths and separation distances. Accordingly, a cross-plot of these dimensions at each of the sampled relay ramps indicates a wide scatter of values (Fig. 9). The best-fit to this scatter suggests an optimum O:S ratio of approximately 4:1, at which ramps breach. This agrees closely with ratios in the range 3:1 to 5:1 typical of breached relay ramps between segments of normal faults surveyed in the Canyonlands National Park, Utah (Mansfield, 1996).

In common with previous compilations, the separation versus overlap data exhibit a considerable spread of values. They indicate that linkage occurred across relay ramps spanning a wide range of aspect ratios, from approximately 1:1 to 1:15. The expected inter-relationship with tip displacements that might rationalise this spread of values is not clear. No unequivocal correlation could be established from any cross-plot of the tip displacement gradients with

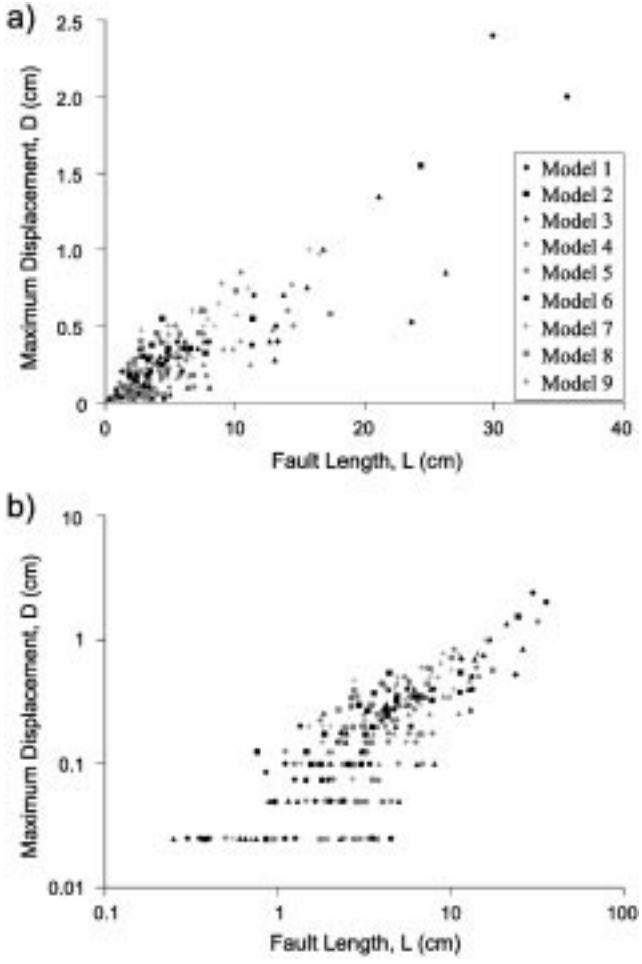

Fig. 10. Maximum Displacement, D versus Fault Length, L data for 237 faults in nine plaster models. The data are plotted on (a) linear, and (b) log–log axes, each with a different symbol according to the model from which it was recorded. Measurement accuracy at the very smallest scales is responsible for the data clustering in b). See main text for discussion.

the associated overlap and separation distances. Huggins et al. (1995) found similar results for the overlapping tips of faults recorded in coalmine plans. They attributed the lack of correlation to the influence of the unconstrained fault structure in three dimensions, i.e. relay ramp geometries evident at one structural level may be preordained by linkage of the fault planes at another. Since movement of the internal wall of our apparatus was driven manually we expect that an additional important variable is the influence of strain rate. Model strain and the transition from ductile folding to brittle faulting at relay ramps probably varied within moderate limits during each modelling run. A final possibility is that mechanical heterogeneity on a scale much smaller than photographically resolvable in the models was responsible for stimulating the propagation of linking structures dissecting the ramps. The random distribution of flaws in the material might in this way dictate specific strain thresholds at which breaching takes place in individual ramps.

The results presented above demonstrate that relay ramps between faults in the plaster models may breach under a wide range of conditions. That is, measurements from the time-lapse photographs suggest that faults overlapping along strike may link for a range of given tip displacement gradients, overlap lengths and separation distances. The absence of any definitive correlation between these variables suggests that ramp breaching is likely to be determined by a complex interplay of all these different measured attributes (Aydin and Schulz, 1990), that cannot be identified by a simple cross-plot of any two.

3.4. Maximum displacement versus fault length

At the end of extension the faults in each model collectively span a wide range of strike lengths (L) and maximum displacements (D). Measurements recorded from 237 separate faults, from all nine models, define a positive correlation between L and D across almost two orders of magnitude (Fig. 10). Regression analysis of these data in log-log space yields a relationship of the form:

$$D = c.L^n \quad (1)$$

where the intercept $c = 0.053$ and the exponent $n = 0.93$. Comparable relationships have been established for similar data recorded from natural fault systems (Walsh and Watterson, 1987; Peacock and Sanderson, 1991; Cartwright et al., 1995, 1996), and the exponent, n, is in close agreement with a theoretically derived value of 1 proposed by Cowie and Scholz (1992a, 1992b).

A striking feature of this data set is the wide scatter of displacement values (Fig. 10). At every fault size there is a spread of between a half and one order of magnitude of D on L and of L on D. Comparable data scatter is a recurring characteristic of D versus L measurements recorded from natural fault arrays and has previously been explained as resulting from the influence of a wide variety of factors. Of these, the most important are believed to be measurement errors and variations in material properties (Walsh and Watterson, 1988; Cowie and Scholz, 1992c). In this instance, measurement errors can safely be disregarded as they are quantifiable and well constrained. Variations in the host material properties may, however, be anticipated as the plaster was hardening during each modelling run. We consider that the effect is negligible for any one single model, as each experiment lasted between 20 and 30 s yet complete solidification of the plaster required at least 1 h. However, because of variations in the precise mix of the plaster and its dependency on ambient temperature, the setting rate during each modelling run will have been significantly different. Since this process is uncontrolled and its impact is poorly understood, we examine the influence of its effect by differentiating the data from each model by plot symbol, in Fig. 10. It is clear from this plot that the range of D and L values spanned by the faults of each model, and their associated scatter of values, are comparable. We therefore conclude that any contrasts in

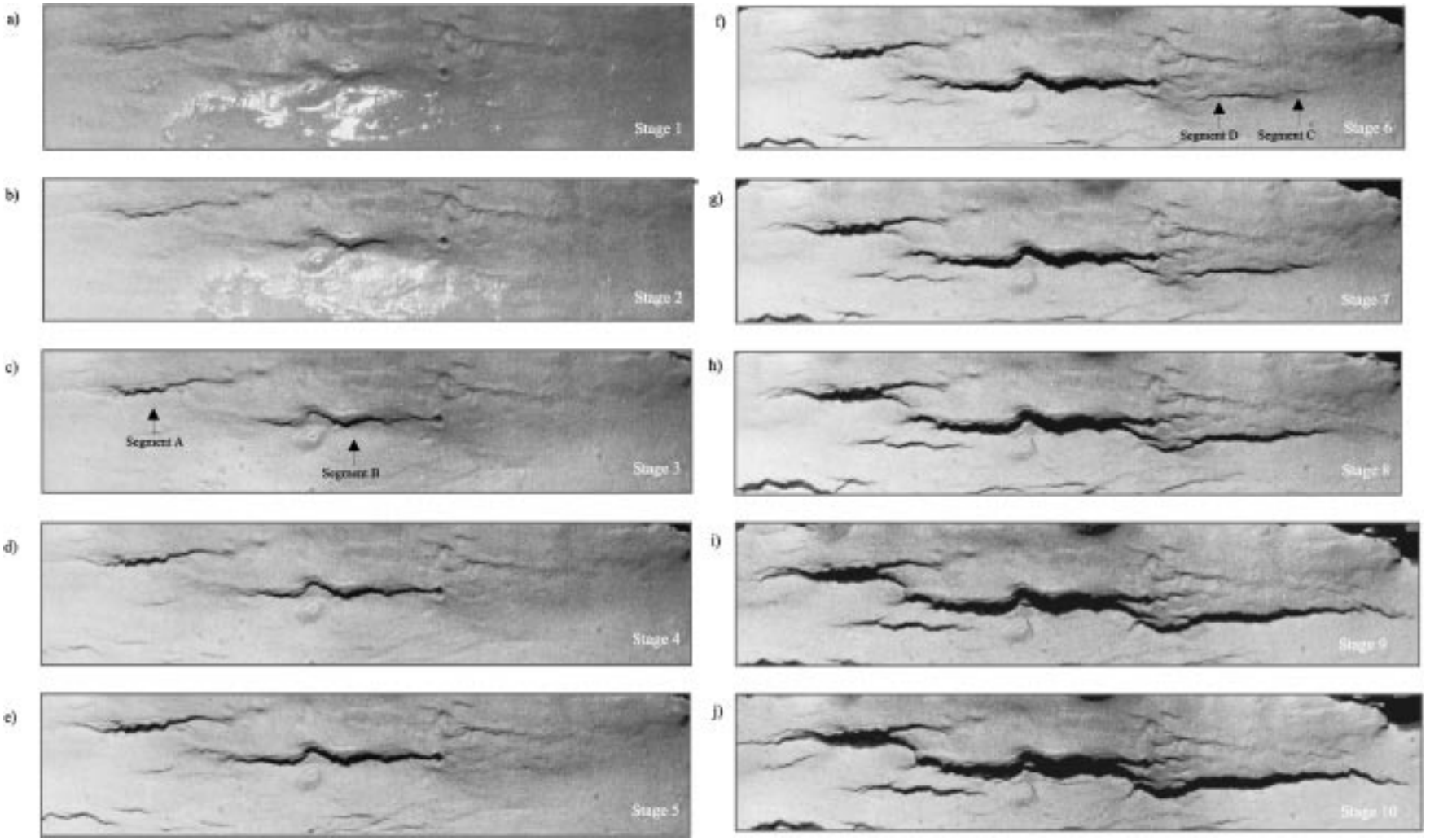

Fig. 11. Sequential, oblique-angle photographs taken during Experiment 38, showing changes to the surface geometry of a fault array at half-second increments during growth. The model is illuminated from the rear (top of photographs) so that the fault planes are cast in shadow. The depth of shadow increases during growth in proportion to displacements on the faults. The fault segment labels A to D are referenced in the main text.

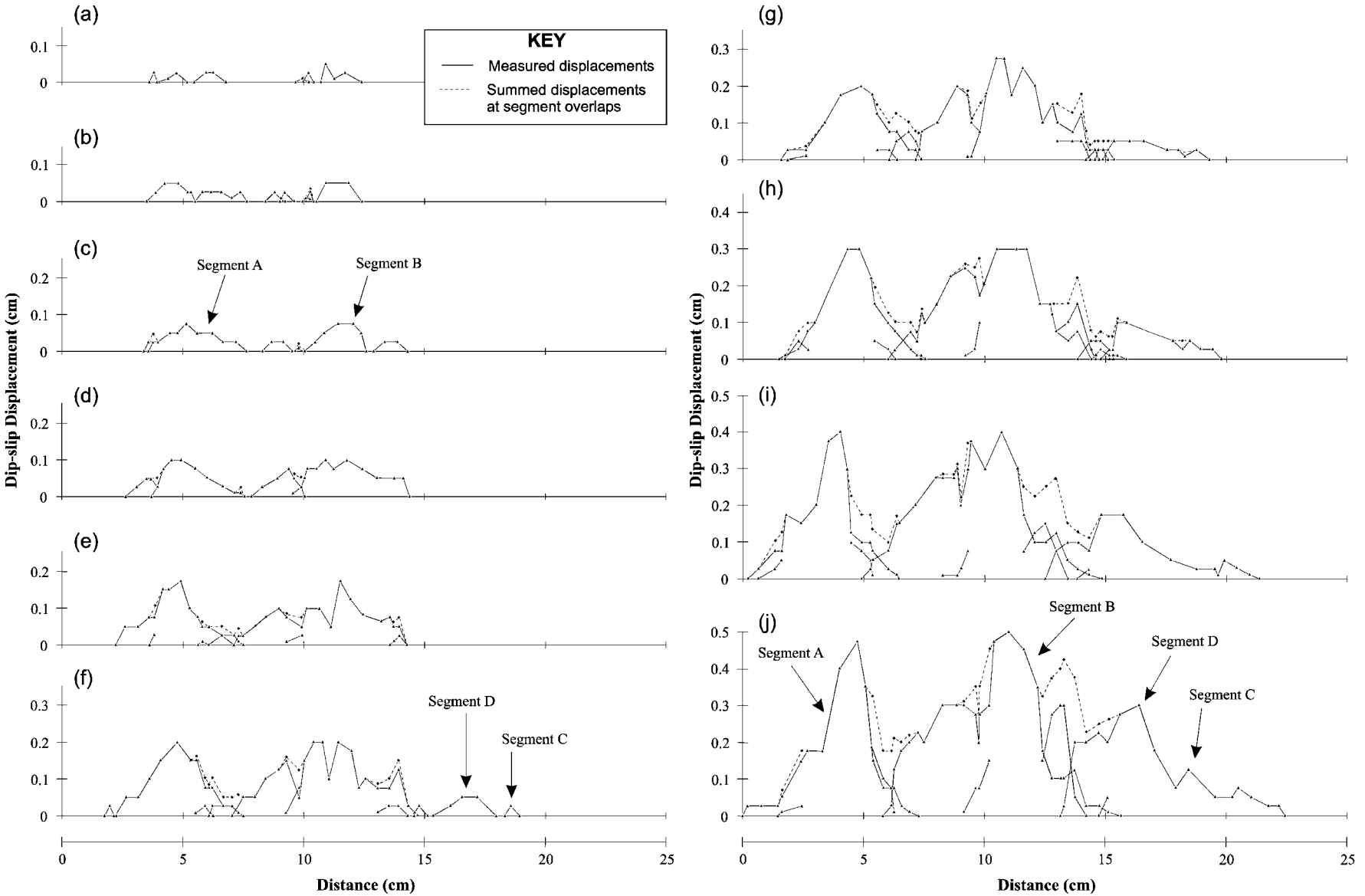

Fig. 12. Sequential strike-parallel displacement profiles for the faults shown in Fig. 11. Solid lines represent the displacements of individual segments and the dashed lines represent cumulative displacements, summed at points of fault segment overlap. Plot symbols at intervals along the strike of the faults indicate individual displacement measurements. The fault segment labels A to D are referenced in the main text

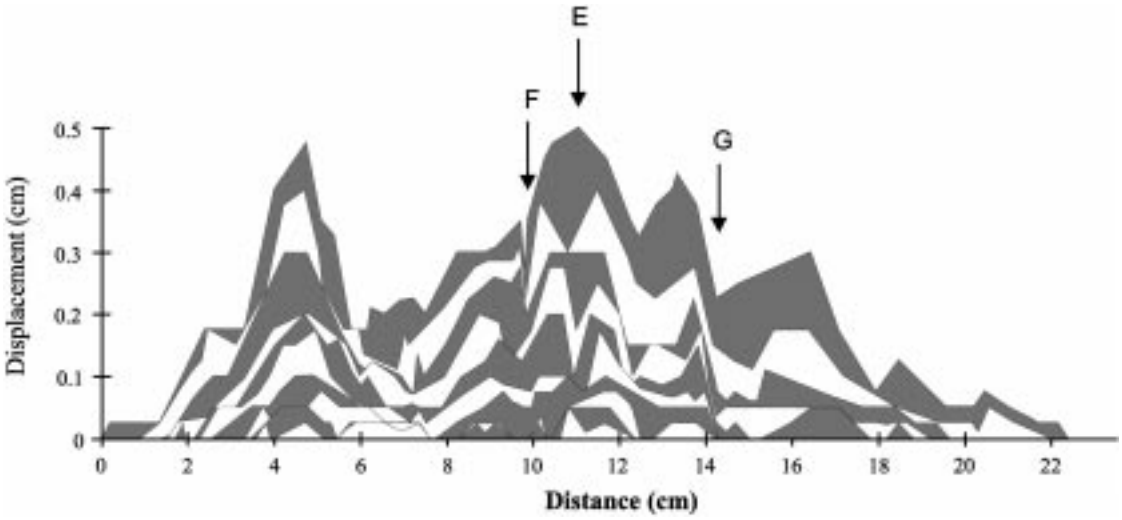

Fig. 13. Composite plot of the displacement profiles shown in Fig. 12. Successive profiles are alternately coloured grey and white in order to emphasise the incremental changes in displacement that occur during the growth of the fault between each of the photograph stages (ref. Fig. 11). The labels E to G indicate characteristic peaks and troughs in the profiles that are discussed in the main text.

plaster rheology between the models has had little discernible effect on the D and L characteristics of the faults. Alternative mechanisms must account for the observed spread of values, and we therefore look to the temporal record of fault development to yield evidence of patterns within the incremental changes in D and L during growth.

3.5. Temporal changes in fault displacements

Reconstructing the incremental growth history of individual faults was made possible in these experiments by using time-lapse photography, providing 'snapshots' of fault development during model extension. These photographs consistently show that growth was in every case governed by a repetitive sequence of tip-line propagation, overlap and linkage with nearest neighbours (Fig. 11). Surface displacements measured along strike therefore define characteristically irregular profiles, fluctuating between local maxima at fault segment centers and minima at segment boundaries (Fig. 12).

Based on changes in displacement during growth, two different linkage styles can be recognised. The first describes connection between the lateral tips of initially isolated segments. A good example of this is illustrated by the coalescence of segments A and B shown in Fig. 11 (c) to (j). The second describes fault nucleation ahead of the expanding tips of an existing segment, as demonstrated by segment C near one tip of segment D in Fig. 11 (f) to (h). Marchal et al. (1999) reported these same two modes of fault linkage, in a recent study of the development of normal faults in sandbox experiments using X-ray tomography.

The former style is representative of accidental linkage, whilst the latter corresponds to incidental linkage, as defined by Childs et al. (1995). This distinction is important, as incidental linkage corresponds to a far greater coherency of cumulative fault displacements during growth than accidental linkage (Fig. 12). Segments A and B (accidental linkage) maintained a strong overprint on the addition of displacement throughout growth of the fault. The two segments overlapped with a prominent cumulative displacement minimum between them, that was maintained during growth despite hard-linkage being established at Stage 9 (Fig. 12 (c) to (j)). Conversely, the cumulative displacement minimum between segments C and D (incidental linkage) was progressively reduced during their mutual growth and overlap (Fig. 12 (f) to (i)). This contrast in post-linkage slip accumulation behaviour has important implications, not least of which is that it possibly affords a means of discriminating between these two modes of linkage (accidental and incidental) in cases where three-dimensional control is absent.

Measurements recorded from the time-lapse photographs lead to the observation that fault growth is governed by contrasting processes operating at two different scales. Firstly, when viewed over several time increments, the growth of individual faults appears constrained by the need to maintain a balance between the addition of displacement and length. This is best illustrated by the preferential accumulation of displacement exhibited by fault segments following hard linkage, often with little or no additional lengthening (e.g. Segments C and D in Fig. 12 (f–h)). In a similar way, local deficits in the addition of displacement on a fault during one time increment appear to have been compensated for during the next increment with extra displacement. Conversely, local displacement maxima observed at one time step were often regions of diminished slip at a later stage. A good illustration of such balanced displacement addition is evident at Point E in Fig. 13, where the amount of slip on the fault alternates between a local maximum and a local minimum during successive time steps. By growing in this way, a broadly uniform

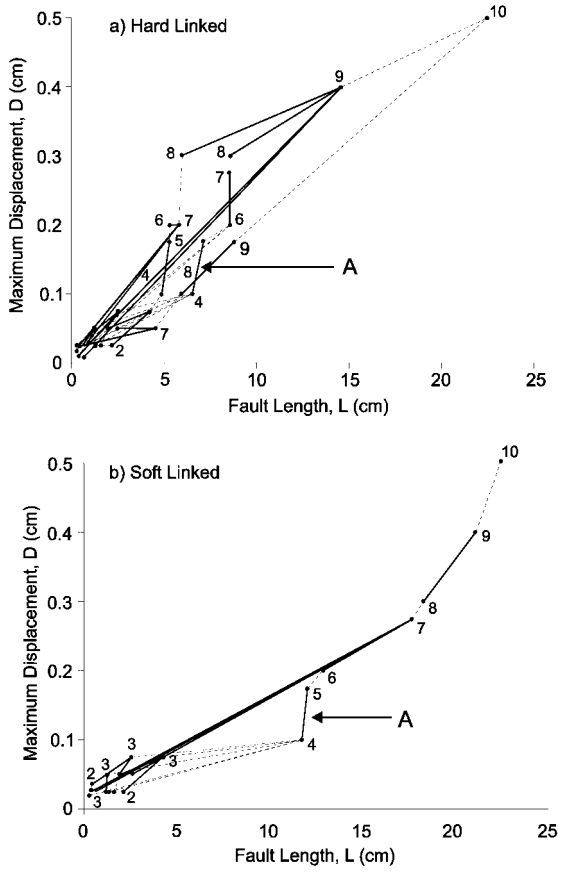

Fig. 14. Scatter plots showing incremental changes in the maximum displacement (D) and length (L) of the fault segments displayed in Fig. 12. The data for each segment are connected alternately by solid and stippled trajectories to emphasise the changes in D and L that occur between each of the measured intervals. The numbers posted adjacent to each trajectory refer to increments in the time-lapse photography (c.f. 'stages' in Fig. 11). They show that irrespective of whether faults are considered connected in either the (a) hard-linked, or (b) soft-linked state, evolution of the array was typified by an appreciable, but variable, scatter of D versus L values.

displacement profile along the strike of the entire fault was maintained during growth (c.f. Fig. 12), increasing from zero at the lateral tips to a maximum close to the centre.

Superimposed on this, however, many fault segments continued to behave as the foci of apparently separate, independent slip distribution long after hard linkage between them. Such behaviour attests to a partial preservation of *kinematic independence* and demonstrates the continued importance of relict segment boundaries (breached relay structures) in governing fault displacement patterns. This is apparent in the many examples of displacement minima that were preserved at fault segment boundaries, despite the continued accumulation of displacement at the adjacent segment centres (e.g. points F and G in Fig. 13). It is in this way that the characteristic short-wavelength 'sawtooth' displacement profile was maintained during significant proportions of the growth interval.

In conjunction with the independent activity of component fault segments, the position of maximum displacement was frequently seen to shift along strike during fault growth. For example, between Stages 4 and 10 (Fig. 12 (d) to (j)) the point of maximum displacement on segment B, measured relative to the model apparatus, fluctuated in position between 10.43 and 11.78 cm along strike. The development of asymmetric displacement distributions during fault segment overlap and interaction commonly also produced *apparent* shifts in the respective displacement maxima, relative to the propagating lateral tips. However, in this example the changes in position were *absolute* within the frame of reference of the model and were governed by the alternating dominance of two neighbouring local maxima. These maxima are separated by a minimum whose position coincides with a pronounced change in fault strike orientation (see Segment B arrow in Fig. 11 (c)) and probably represents an earlier boundary between two smaller segments. Controls governing the preferential growth of one over the other are unclear, but the influence of neighbouring fault segments is thought to have been significant, particularly as a number were active at the lateral tips of both during this interval. Clearly, however, the early segmentation of the fault structure along strike had important consequences for the subsequent distribution of displacement during growth, and largely determined the position of maximum displacement on the fault.

3.6. Temporal changes in maximum displacement and fault length

Incremental changes to the maximum displacement (D) and surface trace length (L) of single faults during growth may be represented in D versus L space as a series of separate 'growth' trajectories. When applied to the growth of the fault segments described above, over the same 5-s time interval, such trajectories describe a series of inclined, divergent and convergent growth paths (Fig. 14).

During growth in isolation, the enlargement of individual fault segments was achieved by propagation of the respective lateral tips simultaneous with the accumulation of displacement over most of the fault surface. In D versus L space, the respective changes in D and L for each of the fault segments define a number of discrete, inclined trajectories. Although similar, these trajectories do not have identical gradients, indicating that individual fault segments increased their lengths and maximum displacements by different proportions.

Conversely, linkage between fault segments during growth is expressed as step-like growth paths, that reflect the irregular increments of length and displacement characteristic of this process (Fig. 14). The individual trajectories of two or more linking faults converge from separate points in D versus L space to meet at positions representing the combined lengths of the segments but only the largest of their maximum displacements. Generally, therefore, linked fault structures are typified by D/L values that are small

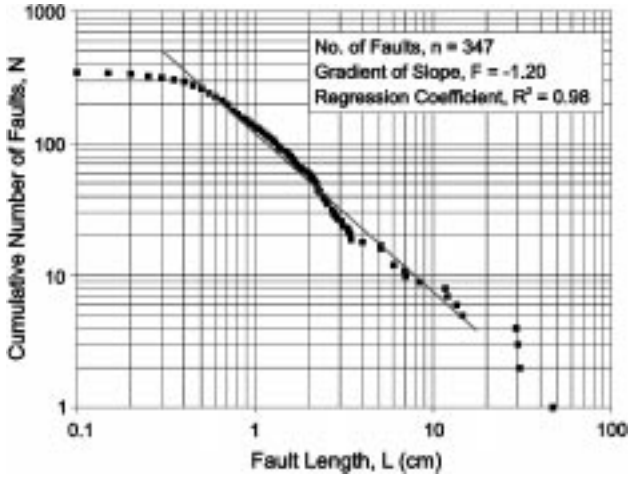

Fig. 15. Population length distribution recorded from 347 faults at the top surface of Model 38, at the end of extension. The regression line shown through the central portion of the data yields a slope for the size-frequency distribution of this fault population of −1.20

relative to those of the component segments (Peacock and Sanderson, 1991; Cartwright et al., 1995). In the absence of further linkage, growth is then typified by an increase in displacement at most points along strike, accompanied only by limited tip-line propagation. Usually, the increase in maximum displacement is proportionally larger than any increase in length. Growth in this interval is therefore represented by trajectories with comparatively steep gradients, defining a return to higher values of D/L. The path highlighted at Position A (Fig. 14 a & b) is a good example. It results first from linkage between small segments at both tips of segment B (Fig. 11 c & d; Fig. 12 c & d), following which growth occurs primarily by the accumulation of displacement.

The growth histories of the individual segments that comprise the final fault structure involve widely different incremental changes to the respective maximum displacement and length parameters. Individual growth trajectories therefore span a range of gradients during the full evolutionary cycle of the fault. These trajectories are almost entirely steeper during growth by tip-line propagation than during growth by linkage, particularly in the interval immediately following linkage. Therefore, although a general trend towards increased values of D and L is evident over the recorded interval, on an incremental basis the growth of individual faults departed appreciably from this trend, irrespective of whether linkage is believed to be established in the soft-linked or the hard-linked state. This point is further emphasised in Fig. 14, where the time-lapse photograph stages shown in Fig. 11 have been posted adjacent to the respective trajectories. It is evident that growth of the entire fault array was characterised by a variable distribution of D/L values through time, governed by the nucleation of new faults and by the propagation and linkage of existing faults.

3.7. Fault size distribution

The size frequency distribution of faults in the plaster models was examined by measuring the lengths of all those faults intersecting the top surface of Model 38. Fault displacement measurements could also have been used for this exercise (e.g. Walsh et al., 1991; Fossen and Gabrielsen, 1996; Wojtal, 1996), but in this case the fault lengths were preferred as they could be measured more precisely.

A total of 347 faults were recorded, their lengths defining the same characteristic tri-segment shape defined by similar data recorded from real fault populations (Fig. 15). Least-squares regression analysis of the central linear part yields a slope for the size frequency distribution of −1.20, which lies between the theoretical limits of −1 and −2 expected for power-law exponents from a 2-D sampling domain (i.e. fault traces measured from one plane in the volume). It is also in good agreement with comparable analyses of certain real fault populations (Yielding et al., 1992, 1996) and is in agreement with fractal dimensions found for other model fault populations (Naylor et al., 1993).

The break of slope with the flatter left-hand portion of the curve is argued to represent either the resolution limit of the applied imaging or measurement technique (Yielding et al., 1992), or is a natural characteristic of the fault population (Walsh and Watterson, 1992). The break of slope occurs in this case (Fig. 15) at 5 mm. Faults of this length were easily resolved by eye and a measurement accuracy of at least 0.5 mm was easily achieved. However, such short microfractures were sufficiently numerous that it is conceivable that not all of them were recorded. In addition, many of the smallest faults may have nucleated at depth and remained entirely blind during subsequent growth.

The steeper right-hand portion of the population curve is much less well defined. It has been argued (e.g. Laslett, 1982) that this represents an edge effect, or 'censoring bias', that arises because faults which intersect the side walls are truncated and therefore assigned lengths that are shorter than they otherwise would have been had the model apparatus been bigger. In this case the population curve indicates the effect is significant for faults with lengths greater than about 28 cm.

4. Discussion

4.1. Displacement distributions along strike

Systematic displacement patterns recognised along the strike of faults in nature have been used previously as a basis for arguing that synonymous with structural connectivity, component segments must also be kinematically linked, for which synchronous growth is necessary (Walsh and Watterson, 1991). The findings of these experiments partially conflict with this idea. Time-lapse photography has confirmed that, when viewed over the complete growth

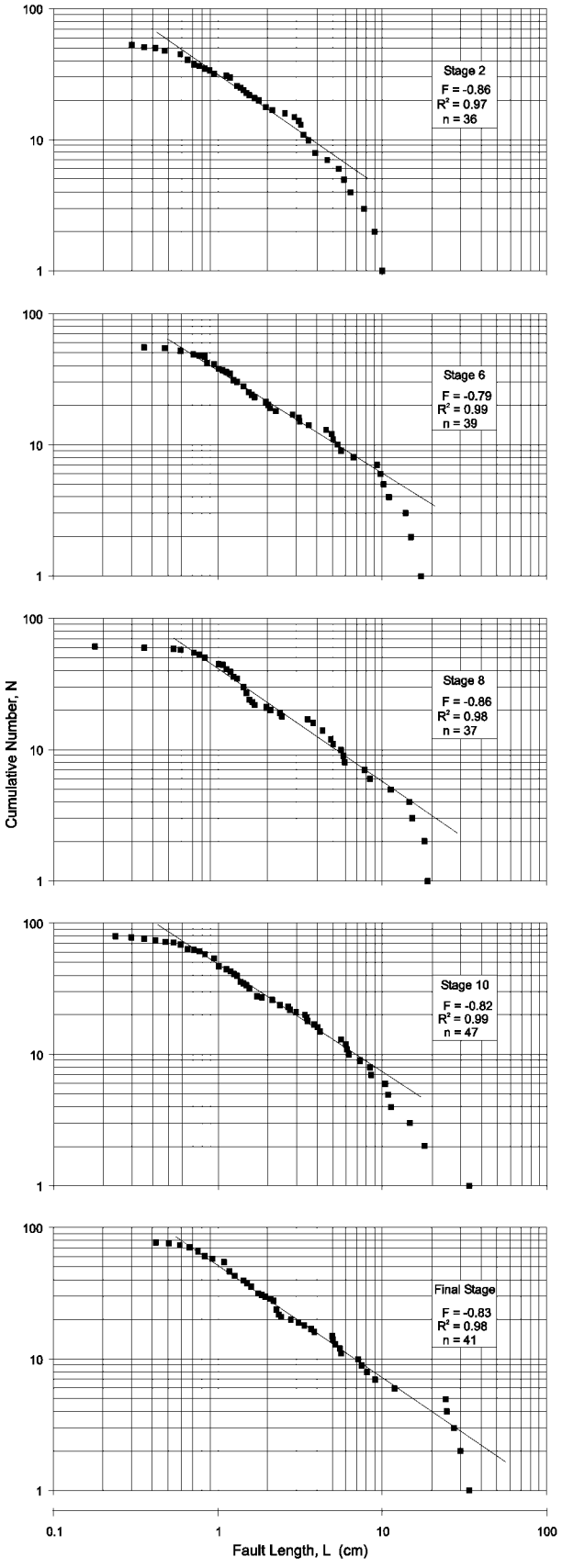

interval, faults do tend towards long-term coherent displacements along strike. However, on an incremental basis, over time scales which are short in relation to the entire growth history of a fault (equivalent, say, to individual slip events), component segments may continue to exhibit independent activity, often for long periods after becoming hard-linked. Good evidence for the sustained separation of individual slip events, in both space and time, is presented by Davison (1995) for two faults in Somerset, UK. The restriction of earthquake ruptures to individual segments of faults is a widely observed phenomenon in seismology (e.g. Machette et al., 1991), and this episodic displacement accumulation through time, that varies along fault strike, is also a general feature of a model for the growth of seismogenic faults presented recently by Cowie (1998). The plaster experiments thus emphasise that linkage of fault segments does not necessarily imply that kinematic harmony will prevail from the moment of linkage onwards during growth.

Where slip is confined to individual segments close to the centre of a fault, such differential displacement accumulation has been shown to result in a simultaneous lateral movement, or a 'migration', of the locus of maximum displacement relative to an external reference such as the model apparatus. However, other shifts in displacement maxima are also frequently observed in conjunction with the growth of segmented faults. For example, propagation of one lateral tip of a fault segment is likely to be arrested or impeded where it relays with a neighbouring segment. Asymmetric displacements will then develop if growth of the other tip continues (e.g. Peacock and Sanderson, 1996). In this case movement of the displacement maximum is purely *apparent*, since only its position relative to both lateral tips changes during growth. If measured relative to the model apparatus, the position of maximum displacement would not actually change. Because segmentation occurs on a number of scales then both types of shift may occur during the growth of any given fault, but discrimination between the two on the basis of displacement data alone is unlikely to be reliable.

4.2. Fault population analysis

Size-frequency plots were established for different intervals in time during each of the modelling experiments (Fig. 16). These plots show that an evolving fault system is typically characterised by distinct and often large fluctuations

Fig. 16. Series of consecutive size-frequency plots showing changes in the length distribution of the fault population in Model 38 at different stages during extension. Fault length measurements were recorded directly from the time-lapse photographs. The annotated stage number refers to the half-second photograph intervals (c.f. Fig. 11). Note the change in the slope of the size-frequency distributions (F), derived from regression of the data, and the change in the data distribution between each stage. See main text for discussion.

in the length distribution of its constituent faults. Through time these changes are the combined product of the increasing size of faults in the population and the nucleation of new faults between each observed interval.

An immediately apparent characteristic of the curves presented in Fig. 16 is the irregularity of the central portions. Steps at certain lengths subdivide the curves into distinct sections, although they do not occur at the same length at each stage. Since the measuring technique applied is the same for all lengths of fault then these steps cannot be attributed to error or systematic differences during the data compilation. Irregularities observed in displacement populations recorded from real faults have previously been explained as resulting from the effects of anisotropy at particular length scales (Wojtal, 1994). However, since in this case the steps do not occur in the same place at each stage then the origin of the effect must only be a transient characteristic of the population at any given length scale.

The steps indicate that within the population there are abrupt increases and decreases in the numbers of faults at particular length scales. One explanation that can be considered to account for this is fault linkage, since the effect numerically is to replace two smaller faults in the population with a larger one at each linkage event. The fluctuating numbers of faults recorded in the population during extension are further evidence that nucleation and linkage were occurring throughout the deformation. Since linkage was a recurrent characteristic of fault evolution it can be expected to have governed changes in the population at every stage during deformation (Filbrandt et al., 1994).

The observation that the 'steps' do not persist at the same lengths from one stage to another suggests that the population somehow readjusts to the changes in the distribution introduced by linkage. This perhaps reflects the initial restrained lengthening of linked faults as they accumulate extra displacement, as previously noted from the recorded changes in D and L (Section 3.4). In this way, the rank of the linked fault in the length distribution of the array would decrease, as others in the population continue to grow. It follows that faults may then 'leapfrog' one another in the length distribution by linkage, but that the bulk distribution is re-established over a period of time as lengthening of the linked faults is checked.

Previously published analogue and numerical modelling data indicate that the onset of significant fault linkage coincided with rapid decreases in the associated length distribution exponent of several studied arrays (Sornette and Davy, 1991; Cowie et al., 1993, 1995; Sornette et al., 1993). The ubiquity of fault linkage during fault development in the plaster models concurs with a tendency towards the preferred lengthening of existing faults and may explain the change in the fractal dimension in this case too.

4.3. Maximum displacement versus fault length

Correlations between maximum displacement and fault length, previously recognised in data recorded from real faults, have been interpreted as representing a controlled scaling of the two variables in the progression towards larger fault structures during array evolution (Watterson, 1986; Walsh and Watterson, 1988; Marrett and Allmendinger, 1991; Cowie and Scholz, 1992c; Gillespie et al., 1992; Dawers et al., 1993; Scholz et al., 1993; Hatton et al., 1994; Schlische et al., 1996). Statistical analyses of the data or equivalent theoretical modelling have attempted to define empirical relationships between D and L that embody this perceived scaling in the progression from small to large faults, i.e. to define a growth sequence.

Despite the appeal of their predictive capabilities, such scaling-law analyses clearly have little application in describing the growth of faults in the plaster models. In the case of fault growth by segment linkage, empirical relationships relating D and L based on the distribution of the data at one particular snapshot in time cannot adequately describe array evolution through time, and neither would they approximate the growth trajectories of individual faults. In this paper we have presented results which confirm the idea that interaction and linkage between faults are responsible for typically irregular, and completely unpredictable, growth paths in D–L space. As seen in the fault growth model presented by Cartwright et al. (1995), the changes in D and L during linkage are largely sequential, not simultaneous. The results of this process are step-like growth trajectories. The exact form of each step is a function of the lengths and the numbers of segments linking at any one time, and the displacements that accrue during and after linkage. The arrest or diminution of ruptures at segment boundaries dictates that growth after linkage may continue to be characterised by intermittent, irregular slip events across a fault plane surface that are separated both in space and time. Consequently, distributions of D versus L data points during array evolution are continually in a state of flux, determined by the numbers and particular linkage state of the component faults through time.

Since there is now overwhelming evidence to suggest that segment linkage was significant in the development of many real faults (Anders and Schlische, 1994; Peacock and Sanderson, 1994; Cartwright et al., 1995, 1996; Dawers and Anders, 1995), it is reasonable to assume that an equally high proportion of scatter in natural D versus L data sets can be accounted for by this mode of growth. This is not to say that other factors, such as variations in material properties, are unimportant for determining the spread of data values. We simply accord them less significance in the light of an almost universal fault growth mechanism that demonstrably contributes to the spread of the model fault data described here.

Most recent studies of fault growth have been typified by an unrelenting preoccupation with defining the trend exhibited by populations of D versus L data, in order to derive an ideal scaling behaviour for fault growth. This, generally, has been at the expense of characterising the distributions as a

whole and of exploring alternative mechanisms to account for the data scatter (i.e. the spread of values and the limits that apparently bound them). It is clear that both the irregular trajectories implicit in growth by segment linkage and the linear trajectories defined by scaling can be accommodated within the typical spread of values characteristic of most D versus L data sets. Without additional constraints, each represents a valid interpretation of the data. However, we have shown here that in any population of faults for which linkage is an integral mechanism of growth, it is clear that the distribution varies through time and that at any one instant in time is a function of the linkage state of the array. Therefore, to prescribe the growth of faults by such definitive scaling relationships is in our view too limiting: it marginalises the significance of the data scatter for representing processes of fault growth. The important corollary to this finding is that erroneous conclusions may therefore be drawn about the manner in which D and L are believed to scale during growth. Other important subsidiary considerations believed to be indicated by the trend or the spread of the data, such as estimates of the in situ shear strength of the host rock (e.g. Cowie and Scholz 1992a), are then likely to be equally in error. Emphasis on scaling behaviour is understandable given the need to derive predictive capability, but it necessarily addresses only the long-term (i.e. over many slip events) relationships between D and L described by the data. For many applications of fault behaviour in which short-term phenomena are important (e.g. earthquakes, dynamic fault seal capacity), the validity of long-term scaling systematics is highly questionable.

5. Conclusions

1. Physical modelling experiments have been described in which gravitational collapse of a two-layer sequence of Crystacal plaster and barite mud has been employed as an analogue for the development of normal faults. The growth of all faults in the models was dominated by repetitive cycles of overlap, relay formation, breaching and linkage between neighbouring segments, across a wide range of scales.

2. Linkage between faults has been shown to have important consequences for patterns of displacement distribution along strike. During growth, most segmented faults were found to exhibit systematic patterns in the long-term accumulation of displacement. However, in contrast, over shorter time-scales component segments of faults were often seen to demonstrate considerable independent activity. This behaviour is believed to arise where segment boundaries persist as asperities to slip, even after physical 'hard-linkage' has been established between faults. In this way local displacement minima remain preserved at segment boundaries. Evidence suggests that this kinematic independence of segments may also be responsible for a lateral re-positioning of the locus of maximum fault displacement at intervals during growth.

3. As first proposed by Cartwright et al. (1995), these experiments have shown that segment linkage is characterised by abrupt and frequently independent changes in maximum displacement and fault length. The effect of this is to cause step-like shapes in the growth trajectories representing the D and L attributes of the respective faults. The magnitude of each step is a function of the size of the linking faults and the number that link at any given instance.

This mechanism is responsible for a considerable proportion of the scatter that characterises the D versus L distributions recorded from the plaster models. Since the progression towards larger structures by coalescence between smaller elements is a phenomenon common to the evolution of many natural fault arrays, we believe that segment linkage must account for a significant proportion of the scatter exhibited by many published D versus L data sets.

4. The rates of change in D and L exhibited by different faults during growth are dependent largely on their own unique history of linkage. Individual faults can exhibit changes in D and L, at different intervals in time, that differ significantly from the trend exhibited by the array as a whole. The disproportionate and independent changes in D and L inherent in growth by segment linkage means that the arrangement of D versus L data points for a given array is in a constant state of flux, depending on the linkage state of that array through time. Consequently, single empirical scaling relationships will never adequately describe the complexity of different D/L ratios exhibited by faults whose growth incorporates linkage between individual segments. They are therefore equally unlikely to accurately reflect the trend that has been described by the data through time.

5. Fault segment linkage has also been shown to have a recognisable effect on the population curve describing the length distribution within a given evolving array. That is, steps or 'gaps' within a population will intermittently appear, resulting from the removal of two faults at smaller length scales and the addition of one combined structure at a much larger scale. However, the populations appear also to be able to readjust to this change. In order to re-establish the characteristic length distribution individual faults will leapfrog one another within the population hierarchy as propagation of the linked faults is temporarily checked.

Acknowledgements

Shell International Petroleum Company Ltd (CSM), Shell Research B.V. and Fina UK Ltd (JAC) are thanked for their financial support of this research. We thank Patience Cowie for many valuable discussions and for reviewing the original manuscript. We also gratefully acknowledge constructive reviews by Peter Cobbold, Haakon Fossen and John Millson.

References

Anders, M.H., Schlische, R.W., 1994. Overlapping faults, intrabasin highs and the growth of normal faults. Journal of Geology 102, 165–180.

Aydin, A., Schulz, R.A., 1990. Effect of mechanical interaction on the development of strike-slip faults with echelon patterns. Journal of Structural Geology 12, 123–129.

Barnett, J.A.M., Mortimer, J., Rippon, J.H., Walsh, J.J., Watterson, J., 1987. Displacement geometry in the volume containing a single normal fault. Bulletin of the American Association of Petroleum Geology 71, 925–937.

Bilham, R., Bodin, P., 1992. Fault zone connectivity: Slip rates on faults in the San Francisco Bay area, California. Science 258, 281–284.

Bürgmann, R., Pollard, D.D., Martel, S., 1994. Slip distributions on faults: effects of stress gradients, inelastic deformation, heterogeneous host-rock stiffness and fault interaction. Journal of Structural Geology 16, 1675–1690.

Cartwright, J.A., Mansfield, C.S., 1998. Lateral displacement variation and lateral tip geometry of normal faults in the Canyonlands National Park, Utah. Journal of Structural Geology 20, 3–19.

Cartwright, J.A., Mansfield, C.S., Trudgill, B.D., 1996. The growth of normal faults by segment linkage. In: Buchanan, P.G., Nieuwland, D.A. (Eds.). Modern Developments in Structural Interpretation, Validation and Modelling. Geological Society Special Publication 99, pp. 163–177.

Cartwright, J.A., Trudgill, B.D., Mansfield, C.S., 1995. Fault growth by segment linkage: An explanation for scatter in maximum displacement and trace length data from the Canyonlands Grabens of SE Utah. Journal of Structural Geology 17, 1319–1326.

Childs, C., Watterson, J., Walsh, J.J., 1995. Fault overlap zones within developing normal fault systems. Journal of the Geological Society of London 152, 535–549.

Cowie, P.A., 1998. A healing-reloading feedback control on the growth rate of seismogenic faults. Journal of Structural Geology 20, 1075–1087.

Cowie, P.A., Scholz, C.H., 1992a. Physical explanation for displacement-length relationship for faults using a post-yield fracture mechanics model. Journal of Structural Geology 14, 1133–1148.

Cowie, P.A., Scholz, C.H., 1992b. Growth of faults by accumulation of seismic slip. Journal of Geophysical Research 97, 11085–11096.

Cowie, P.A., Scholz, C.H., 1992c. Displacement-length scaling relationship for faults: Data synthesis and discussion. Journal of Structural Geology 14, 1149–1156.

Cowie, P.A., Shipton, Z.K., 1998. Fault tip displacement gradients and process zone dimensions. Journal of Structural Geology 20, 983–997.

Cowie, P.A., Sornette, D., Vanneste, C., 1995. Multifractal scaling properties of a growing fault population. Geophysical Journal International 122, 457–469.

Cowie, P.A., Vanneste, C., Sornette, D., 1993. Statistical physics model for the spatio-temporal evolution of faults. Journal of Geophysical Research 98, 21809–21821.

Davison, I., 1995. Fault slip evolution determined from crack-seal veins in pull-aparts and their implications for general slip models. Journal of Structural Geology 17, 1025–1034.

Dawers, N.H., Anders, M.H., 1995. Displacement-length scaling and fault linkage. Journal of Structural Geology 17, 607–614.

Dawers, N.H., Anders, M.H., Scholz, C.H., 1993. Growth of normal faults: Displacement-length scaling. Geology 21, 1107–1110.

Filbrandt, J.B., Richard, P.D., Franssen, R.C.M.W., 1994. Growth and coalescence of faults: Numerical simulations and sandbox experiments. Extended Abstracts of Proceedings, Fault Populations Conference, University of Edinburgh, pp. 57–59.

Fossen, H., Gabrielsen, R.L., 1996. Experimental modeling of extensional fault systems by use of plaster. Journal of Structural Geology 18, 673–687.

Gillespie, P.A., Walsh, J.J., Watterson, J., 1992. Limitations of dimension and displacement data from single faults and the consequences for data analysis and interpretation. Journal of Structural Geology 14, 1157–1172.

Gudmundsson, A., 1987a. Tectonics of the Thingvellir fissure swarm, SW Iceland. Journal of Structural Geology 9, 61–69.

Gudmundsson, A., 1987b. Geometry, formation and development of tectonic fractures on the Reykjanes Peninsula, southwest Iceland. Tectonophysics 139, 295–308.

Hatton, C.G., Main, I.G., Meredith, P.G., 1994. Non-universal scaling of fracture length and opening displacement. Nature 367, 160–162.

Horsfield, W.T., 1977. An experimental approach to basement-controlled faulting. Geologie en Mijnbouw 56, 363–370.

Hubbert, M.K., 1937. Theory of scale models as applied to geologic structures. Bulletin of the Geological Society of America 48, 1459–1520.

Huggins, P., Watterson, J., Walsh, J.J., Childs, C., 1995. Relay zone geometry and displacement transfer between normal faults recorded in coal-mine plans. Journal of Structural Geology 17, 1741–1755.

Lachenbruch, A.H., 1962. Mechanics of thermal contraction cracks and ice-wedge polygons in permafrost. Geological Society of America Special Paper 70, 69pp.

Laslett, G.M., 1982. Censoring and edge effects in areal and line transect sampling of rock joint traces. Journal of the International Association of Mathematical Geology 14, 125–140.

Machette, M.N., Personius, S.F., Nelson, A.R., Schwarz, D.P., Lund, W.R., 1991. The Wasatch fault zone, Utah: Segmentation and history of Holocene earthquakes. Journal of Structural Geology 13, 137–149.

Mansfield, C.S. 1996. Fault growth by segment linkage. Unpublished Ph.D thesis, University of London. 291pp.

Marchal, D., Guiraud, M., Rives, T., van den Driessche, J., 1999. Space and time propagation processes of normal faults. In: Jones, G., Fisher, Q.J., Knipe, R.J. (Eds.). Faulting, Fault Sealing and Fluid Flow in Hydrocarbon Reservoirs. Geological Society Special Publication 147, pp. 51–70.

Marrett, R., Allmendinger, R.W., 1991. Estimates of strain due to brittle faulting: sampling of fault populations. Journal of Structural Geology 13, 735–738.

McClay, K.R., Ellis, P.G., 1987. Geometries of extensional fault systems developed in model experiments. Geology 15, 341–344.

Naylor, M.A., Mandle, G., Slijpesteijn, C.H.K., 1986. Fault geometries in basement-induced wrench faulting under different initial stress states. Journal of Structural Geology 8, 737–752.

Naylor, M.A., Larroque, J.M., Gauthier, B.D.M. 1993. Understanding extensional tectonics: Insights from sandbox models. Shell Research Document, Publication 1144, Shell Internationale Research Mij. B.V., 11pp.

Nelson, R.A., Patton, T.L., Morley, C.K., 1992. Rift segment interaction and its relation to hydrocarbon exploration in rift systems. Bulletin of the American Association of Petroleum Geologists 76, 1153–1169.

Nicol, A., Watterson, J., Walsh, J.J., Childs, C., 1996. The shapes, major axis orientations and displacement patterns of fault surfaces. Journal of Structural Geology 18, 235–248.

Oertel, G., 1965. The mechanism of faulting in clay experiments. Tectonophysics 2, 343–393.

Peacock, D.C.P. 1995. Mapping small faults-why size is not important. Geoscientist 5, #2, 28-30.

Peacock, D.C.P., Sanderson, D.J., 1991. Displacements, segment linkage and relay ramps in normal fault zones. Journal of Structural Geology 13, 721–733.

Peacock, D.C.P., Sanderson, D.J., 1994. Geometry and development of relay ramps in normal fault systems. Bulletin of the American Association of Petroleum Geologists 78, 147–165.

Peacock, D.C.P., Sanderson, D.J., 1996. Effects of propagation rate on displacement variations along faults. Journal of Structural Geology 18, 311–320.

Pollard, D.D., Segall, P., 1987. Theoretical displacements and stresses near fractures in rock: with applications to faults, joints, veins, dykes and solution surfaces. In: Atkinson, B. (Ed.). Fracture Mechanics of Rock, Academic Press, London, pp. 277–349.

Ramsay, J.G., Huber, M.I., 1987. The Techniques of Modern Structural Geology, Academic Press Inc. (London) Limited, London, p. 700.

Sales, J.K., 1987. Tectonic models. In: Seyfert, C.K. (Ed.). Encyclopedia of Structural Geology and Tectonics, Van Nostrand Reinhold, New York, pp. 785–794.

Schlische, R.W., Young, S.S., Ackermann, R.V., Gupta, A., 1996. Geometry and scaling relations of a population of very small rift-related normal faults. Geology 24, 683–686.

Scholz, C.H., Dawers, N.H., Yu, J.-Z., Anders, M.H., Cowie, P.A., 1993. Fault growth and fault scaling laws: Preliminary results. Journal of Geophysical Research 98, 21951–21961.

Sornette, D., Davy, P., 1991. Fault growth model and the universal fault length distribution. Geophysical Research Letters 18, 1079–1081.

Sornette, A., Davy, P., Sornette, D., 1993. Fault growth in brittle-ductile experiments and the mechanics of continental collisions. Journal of Geophysical Research , 12,111-12 98, 139.

Tchalenko, J.S., 1970. Similarities between shear zones of different magnitudes. Bulletin of the Geological Society of America 81, 1625–1639.

Trudgill, B.D., Cartwright, J.A., 1994. Relay ramp forms and normal fault linkages-Canyonlands National Park, Utah. Bulletin of the Geological Society of America 106, 1143–1157.

Vendeville, B., Cobbold, P.R., Davy, P., Bruhn, J.P., Choukroune, P., 1987. Physical models of extensional tectonics at various scales. In: Coward, M.P., Dewey, J.F., Hancock, P.L. (Eds.). Continental Extensional Tectonics. Geological Society Special Publication 28, pp. 95–107.

Walsh, J.J., Watterson, J., 1987. Distribution of cumulative displacement and seismic slip on a single normal fault surface. Journal of Structural Geology 9, 1039–1046.

Walsh, J.J., Watterson, J., 1988. Analysis of the relationship between displacements and dimensions of faults. Journal of Structural Geology 10, 239–247.

Walsh, J.J., Watterson, J., 1991. Geometric and kinematic coherence and scale effects in normal fault systems. In: Roberts, A.M., Yielding, G., Freeman, B. (Eds.). The Geometry of Normal Faults. Geological Society Special Publication 56, , pp. 193–203.

Walsh, J.J., Watterson, J., 1992. Populations of faults and fault displacements and their effects on estimates of fault-related regional extension. Journal of Structural Geology 14, 701–712.

Walsh, J.J., Watterson, J., Yielding, G., 1991. The importance of small-scale faulting in regional extension. Nature 351, 391–393.

Watterson, J., 1986. Fault dimensions, displacements and growth. Pure and Applied Geophysics 124, 365–373.

Willemse, E.J.M., Pollard, D.D., Aydin, A., 1996. Three-dimensional analyses of slip distributions on normal fault arrays with consequences for fault scaling. Journal of Structural Geology 18, 295–309.

Wojtal, S.F., 1994. Fault scaling laws and the temporal evolution of fault systems. Journal of Structural Geology 16, 603–612.

Wojtal, S.F., 1996. Changes in fault displacement populations correlated to linkage between faults. Journal of Structural Geology 18, 265–280.

Yielding, G., Walsh, J.J., Watterson, J., 1992. The prediction of small scale faulting in reservoirs. First Break 10, 449–460.

Yielding, G., Needham, T., Jones, H., 1996. Sampling of fault populations using sub-surface data: a review. Journal of Structural Geology 18, 135–146.